lubricants

MDPI

Article

Tribological and Corrosion Effects from Electrodeposited Ni-hBN over SS304 Substrate

Suresh Velayudham [1], Elango Natarajan [2,*], Kalaimani Markandan [2], Kaviarasan Varadaraju [1], Santhosh Mozhuguan Sekar [3], Gérald Franz [4,*] and Anil Chouhan [2]

[1] Department of Mechanical Engineering, Sona College of Technology, Salem 636005, India; catsuresh@gmail.com (S.V.); vkavi.cim@gmail.com (K.V.)
[2] Faculty of Engineering, Technology and Built Environment, UCSI University, Kuala Lumpur 56000, Malaysia; kalaimani@ucsiuniversity.edu.my (K.M.); 1002161329@ucsiuniversity.edu.my (A.C.)
[3] Department of Mechanical Engineering, Selvam College of Technology, Namakkal 637003, India; mozhuguan.santhosh@gmail.com
[4] Laboratoire des Technologies Innovantes, UR UPJV 3899, Avenue des Facultés, Le Bailly, 80025 Amiens, France
* Correspondence: elango@ucsiuniversity.edu.my (E.N.); gerald.franz@u-picardie.fr (G.F.)

Abstract

The aim of the present study is to investigate the influence of Nickel–Hexagonal Boron Nitride (Ni-hBN) nanocomposite coatings, deposited using the pulse reverse current electrodeposition technique. This experimental study focuses on assessing the tribological and corrosion properties of the produced coatings on the SS304 substrate. The microhardness of the as-deposited (AD) sample and heat-treated (HT) sample were 49% and 83.8% higher compared to the control sample. The HT sample exhibited a grain size which was approximately 9.7% larger than the AD sample owing to the expansion–contraction mechanism of grains during heat treatment and sudden quenching. Surface roughness reduced after coating, where the Ni-hBN-coated sample measured a roughness of 0.43 µm compared to 0.48 µm for the bare surface. The average coefficient of friction for the AD sample was 42.4% lower than the bare surface owing to the self-lubricating properties of nano hBN. In particular, the corrosion rate of the AD sample was found to be 0.062 mm/year, which was lower than values reported in other studies. As such, findings from the present study can be particularly beneficial for applications in the automotive and aerospace industries, where enhanced wear resistance, reduced friction, and superior corrosion protection are critical for components such as engine parts, gears, bearings and shafts.

Keywords: pulse reverse electrodeposition; heat treatment; hBN; corrosion; wear; product innovation; sustainable manufacturing

check for updates

Received: 19 June 2025
Revised: 19 July 2025
Accepted: 20 July 2025
Published: 21 July 2025

Citation: Velayudham, S.; Natarajan, E.; Markandan, K.; Varadaraju, K.; Mozhuguan Sekar, S.; Franz, G.; Chouhan, A. Tribological and Corrosion Effects from Electrodeposited Ni-hBN over SS304 Substrate. *Lubricants* **2025**, *13*, 318. https://doi.org/10.3390/lubricants13070318

Copyright: © 2025 by the authors. Licensee MDPI, Basel, Switzerland. This article is an open access article distributed under the terms and conditions of the Creative Commons Attribution (CC BY) license (https://creativecommons.org/licenses/by/4.0/).

1. Introduction

The 304 stainless steel, also known as SS304, has been widely used in many engineering applications due to its ductility, toughness, high hardness, weldability, wear resistance, corrosion resistance, and pleasing aesthetic effects [1]. Despite its high corrosion resistance, the coating may be amended to increase its durability and adaptability to a wide range of environmental services. To this end, electrodeposition has appeared to be a versatile technique to economically produce a coated metal matrix composite (MMC) where second-phase elements are employed for the coating [2]. For instance, Gyawali et al. [3] conducted an hBN nano sheet coating on Ni plate using a sulfamate electrolytic bath. Bouzit et al. [4]

and Khorsand et al. [5] conducted a Co-Ni coating using a chloride–sulfate bath and NaCl bath, respectively. Zhang et al. [6] conducted a Ni coating using the droplet contact method whereby the coating was performed layer by layer. The advantage of the droplet contact electrodeposition method is that it has a superior liquid-phase mass transfer effect. Bigos et al. [7] conducted a Mo-Co coating on a steel substrate where they used citrate electrolyte medium and annealing heat treatment.

Various current modes, including direct current, pulse current, and pulse reverse current, exert distinct influences on the nano-crystallized surfaces of coatings with additives. Single-pulse electrodeposition under pulse current mode achieves superior control over grain size, surface morphology, and orientation compared to direct current. While pulse-reverse current electrodeposition (PRED) enhances thickness distribution, mitigates hydrogen embrittlement, activates surfaces, and produces smoother, denser coatings with decreased porosity and a traditional electrochemical deposition induces hydrogen bubble formation near the cathode, impeding ion throughput. To overcome this challenge, electrochemical deposition with a pulse input has been utilized for the coating [8]. Bucur et al. [9] coated hydroxyapatite on a Ti substrate for improving its properties, where they found that crystals of hydroxyapatite were uniformly organized into hemispheres and the coating appeared with two layers: a uniform base layer and upper layer formed by longer deposition with lower density. Tohidi et al. [10] coated calcium phosphate over a NiTi plate for modifying the surface condition of this shape memory alloy. In a NiTi implant, the release of toxic Ni ions hinders the use of NiTi for the human body and hence this research was conducted with hydroxyapatite which has a Ca/P ratio similar to human bone.

In this deposition method, the time between unipolar pulses can reduce hydrogen emission and promote ion diffusion, resulting in an enhanced ion concentration at the cathode surface. Thus, pulsed cathodic electrochemical deposition can yield uniform coatings with low porosity. Additionally, pulse reverse power enhances coating adhesion by promoting the growth of adherent particles from the coated layer [11,12]. Li et al. [13] proposed a hybrid coating method where a laser was used to self-assemble SiC nanoparticles onto a porous structure of steel substrate. The coated sample was exposed to air for a period to change the wettability of the surface aligning to superhydrophobicity. PRED reduces diffusion layer thickness, enhances cathodic current efficiency, and accelerates coating deposition, yielding zinc coatings with superior corrosion resistance to pulse electrodeposition. It is an innovative technique capable of creating unique nanostructures in alloys, metal oxides, and metals, offering precise modification of their physicochemical and structural traits [14,15].

Mandich's findings demonstrate that modifying PRED parameters significantly impacts electrodeposit properties, disrupting adsorption and desorption processes, and altering diffusion layer thickness. Researchers are actively harnessing PRED's potential to enhance materials' structural and physicochemical traits. Functioning akin to a bipolar electrodeposition process, PRED's continuous switch between anodic and cathodic periods drives its theoretical framework [16]. Nickel-coated composites have received much attention in the last three decades because of their exceptional characteristic performance [17]. In recent years, studies have focused on the electrodeposition process with second-phase elements such as oxides (TiO_2, Al_2O_3, ZrO_2, Cr_2O_3, Fe_2O_3), carbides (SiC, WC, TiC), nitrides (Si_3N_4, TiN), and two-dimensional elements such as graphene, hBN, germanene, and MWCNT [18–38]. Among the various second-phase elements, hBN has gained significant research as it possesses excellent thermal and electrical conductivity, and high mechanical and tribological characteristics. Because of these excellent properties, hBN is also referred to as white graphene [39].

Numerous researchers have conducted a Ni-hBN composite coating due to enhanced friction, wear properties, and corrosion resistance. A recent study by Zuo et al. demonstrated a nano hBN coating on a stainless-steel wire cloth that constitutes superior characteristics to the adaptable electrothermal heating and supports desalinate hypersaline solutions [40]. Readers can refer to the literature for topics like electroless coating [41], electrophoretic coating [42], and electrodeposition coating [43] to understand how input parameters such as frequency, duty cycle, and current density on the deposition of particles are important. Ahmadkhaniha et al. [44] investigated the effect of post-heating of Ni-P-SiC at 400 °C for an hour and reported that post-heating (with annealing and tempering) was desirable to enhance surface properties. Kiran et al. [45] and Jiang et al. [46] also asserted the importance of the post-treatment of composite coatings in their publication on Ni–P–BN(h) composite coatings and Ni–P–GO composite coatings, respectively.

The main objective of this research is to enhance the mechanical properties, specifically microhardness, wear resistance, and corrosion resistance of Ni-hBN nanocomposite coatings applied to SS304 stainless-steel substrates, both with and without oil quenching. While several studies have investigated the effectiveness of pulsed and pulse-reverse electrodeposition techniques for Ni-based coatings, limited research has focused on Ni-hBN nanocomposite coatings combined with post-deposition heat treatment involving oil quenching. This study aims to explore the potential of such coatings as a viable alternative to hard chrome plating, offering improved corrosion resistance with minimal hardness requirements.

In this work, Section 2 details the materials used and the in situ experimental procedures, including the electrodeposition of Ni-hBN nanocomposites on SS304 substrates and subsequent heat treatment using SAE 40 grade oil for quenching. Section 3 presents and discusses the investigation and analysis of key mechanical and surface properties, including microhardness, grain crystal size, surface roughness, wear resistance, and corrosion resistance, along with their corresponding results.

2. Experimental Procedure

2.1. Materials and Preparation of Samples

SS304 ingot size of 2440 mm was purchased from the local supplier and cut into substrates according to ASTM G99 standards [47]. These substrate samples were cylindrical with a diameter ∅ = 10 mm and a length of 30 mm, which comply with ASTM standards. It was first grounded using sandpapers having grit sizes of 200#, 600#, and 1200# to eliminate oxide film from the surface and obtain a bright surface, followed by velvet cloth cleaning to remove scratches from the surface. The surfaces were later cleaned using distilled water, followed by cleaning with 0.5 M H_2SO_4 and 0.5 M HCl for 20 s. These were conducted to mend the better bond between the substrate and coating material.

Hexagonal boron nitride (hBN) nano powders (size < 50 nm) were purchased from Platonic Nanotech Private Limited. All the chemicals (Ni sulphate, Ni chloride, and Boric acid) were purchased from Merck brand, Germany. Firstly, the electrolyte of 300 mL was prepared in a 500 mL beaker and stirred continuously for 24 h at 400 rpm using a magnetic stirrer. Before coating, the electrolyte was agitated using an ultrasonic agitator for 30 min to avoid cloud formation. Before preparing actual samples, trail experiments were performed with different parameters, and the coating was examined using an optical microscope. Once optimal setting parameters were confirmed as listed in Table 1, actual samples were prepared.

Table 1. Chemicals used and operating conditions in the preparation of Ni–hBN-coated SS304 samples.

Chemicals Used	Operating Condition
Nickel sulfate (250 g/L, pH = 4 ± 0.2) Nickel chloride (40 g/L) Boric acid (30 g/L) Sodium Dodecyl Sulfate SDS (0.1 g/L)	Mixing speed: 400 rpm Deposition time: 300 s Frequencies: 10 Hz, 20 Hz, and 30 Hz Temperature: 55 ± 2 °C [10] Duty cycles: 10%, 20%, and 30% Polarity ratio: 2

The setting parameters were computed as explained below.

$$\text{Total time: } T = T_{on(for)} + T_{off(for)} + T_{on(rev)} + T_{off(rev)} \quad (1)$$

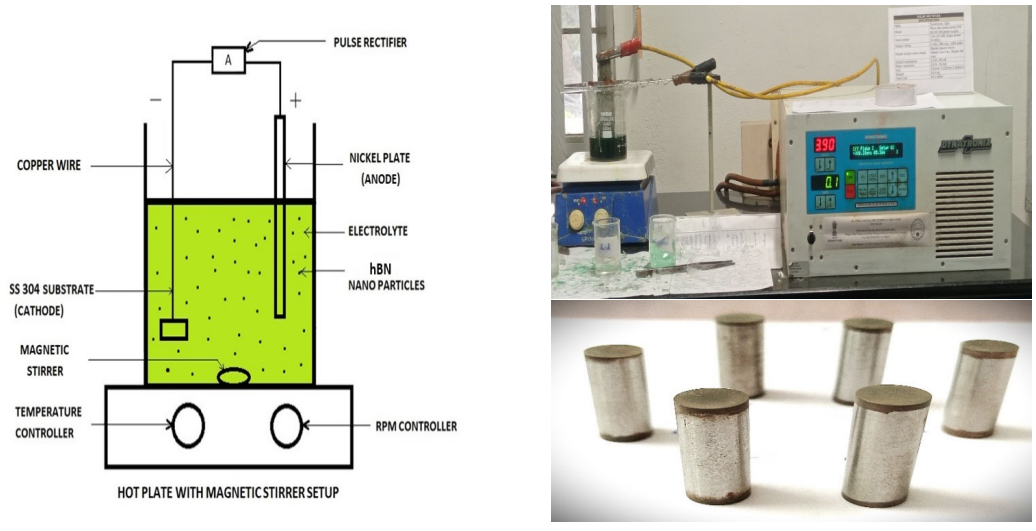
$$\text{Average current density: } i_m = \frac{\left(i_a \; x \; T_{on(for)} \; - i_b \; x \; T_{on(rev)}\right)}{T} \quad (2)$$

$$\text{Positive duty cycle: } t_{d(for)} = \frac{T_{on(for)}}{T_{on(for)} + T_{off(for)}} \quad (3)$$

$$\text{Reverse duty cycle: } t_{d(rev)} = \frac{T_{on(rev)}}{T_{on(rev)} + \; T_{off(rev)}} \quad (4)$$

where $T_{on(for)}$ and $T_{on(rev)}$ represent positive and negative pulse lengths while $T_{off(for)}$ and $T_{off(rev)}$ are positive and negative relaxation periods. All these terms are expressed in ms. i_a, i_b, and i_m depict positive peak, negative peak, and average current densities and are given in A/cm^2.

Figure 1 depicts PRED setup and Ni–hBN-coated SS304 samples. Herein, these samples are referred to as-deposited (AD) samples throughout the paper. The coated samples were later cleaned in distilled water to remove loosely absorbed nanoparticles from the surface. The post-heat treatment of coated samples was performed at 400 °C for an hour [18] followed by a rapid quenching using SAE 40 grade oil. Three samples at the same condition were prepared to ensure repeatability. Herein, these heat-treated samples are referred as heat-treated (HT) samples.



(**a**) (**b**)

Figure 1. Pulse-Reverse Electrodeposition of Ni–hBN composite coating: (**a**) schematic setup; (**b**) experimental device and coated samples.

2.2. Mechanical Properties and Characterizations

Field emission scanning electron microscopy (FESEM, model: Zesis, Oberkochen, Germany), energy dispersive X-ray spectrometry (EDX, model: Bruker, Billerica, MA, USA), and X-ray diffraction (XRD, PAN analytical Philips X'Pert Pro diffractometer, PANalytical, Malvern, UK) were used to characterize surface morphologies, microstructures, and the chemical composition of the coated films with Cu K-α radiation (the X-ray wavelength is λ = 1.542 Å). The data were obtained over a 2θ scan range of 10–90°, with a step size of 0.0130° and scan time of 0.5 s. The average size d of crystallites was calculated using the Debye–Scherrer equation $d = \frac{k\lambda}{\beta cos\theta}$ [48]. The hardness of the AD and HT samples was determined using a Vickers microhardness tester (Model: Shimaduzu HMG-G31ST, Kyoto, Japan). The following test conditions were used: a load of 50 g was applied and maintained during a holding time of 15 s; five indentations per sample were performed and averaged. Surface roughness of the coated samples was measured using a surface profilometer, while coating thickness was measured using Metallurgical Microscope-OIAL/MMN/MET/01 according to ISO 1463:2004 standards [49] at a room temperature condition with a 1500X magnification.

The wear and friction behavior of the AD and HT samples were assessed using a pin-on-disk tribometer, DUCOM (TR-201CL). This dry sliding test was performed against EN31 steel under room temperature for a sliding distance of 1000 mm with a track diameter of 60 mm. Wear resistance was measured while the pin was applied with a load of 20 N at the sliding velocity of 1.64 m/s. The corrosion resistance of the AD and HT coatings were measured using electrochemical impedance spectroscopy as per the ASTM G106-89 standard [50] (EIS-CHI-650C, USA electrochemical workstation), which utilizes the polarization technique (Tafel plot). It had three-electrode cells; the counter electrode (platinum foil) where measurement was taken, the reference electrode which is a saturated calomel electrode (SCE), and working electrode which is the coated surface. The surface area with a 5 mm radius was exposed in the test solution consisting of 3.5% NaCl corrosive medium. An EIS test was performed with a frequency ranging from 0.1 Hz to 1×10^5 Hz with an amplitude of 10 mV at open circuit potential. Open circuit potential was carried out ranging from −500 mV to +500 mV in NaCl, followed by an electrochemical impedance spectroscopy measurement. The potentiodynamic polarization was performed in the range from −500 mV below OCP to +500 mV above OCP at a scan rate of 0.5 mV/s. The results of this investigation are presented in the following section.

3. Results and Discussion

The aim of this research was to investigate the effect of a Ni-hBN composite coating and evaluate the performance of a heat-treated Ni-hBN composite coating. Hence, topography and microstructure of AD samples and HT samples were examined and analyzed using FESEM and EDX studies. Figure 2a–d shows the surface morphology of Ni–hBN coated samples at 1 µm, 2 µm, 100 nm, and 200 nm magnifications. Under the magnification 1 µm and 2 µm, we found the appearance of Ni-hBN in a flake-like structure and some cylindrical structures as shown in Figure 2a,b. Upon magnifying the surface further at 100 µm, vivid cylindrical-shaped Ni-hBN was observed. Agglomerated particles were also visible as shown in Figure 2d. However, the more uniform and denser Ni-hBN coating was observed from these SEM examinations. The reason for the uniform coating was since the pulse-reverse current dissolves the large grain size particles to make the surface smoother. From the elemental composition analysis given by EDX in Figure 2e, it was noticed that the coated sample primarily has the nickel (Ni) element (86.15% of its total weight), followed by boron (B) (13.42%), and remaining elements of nitrogen (N) (0.42 wt.%).

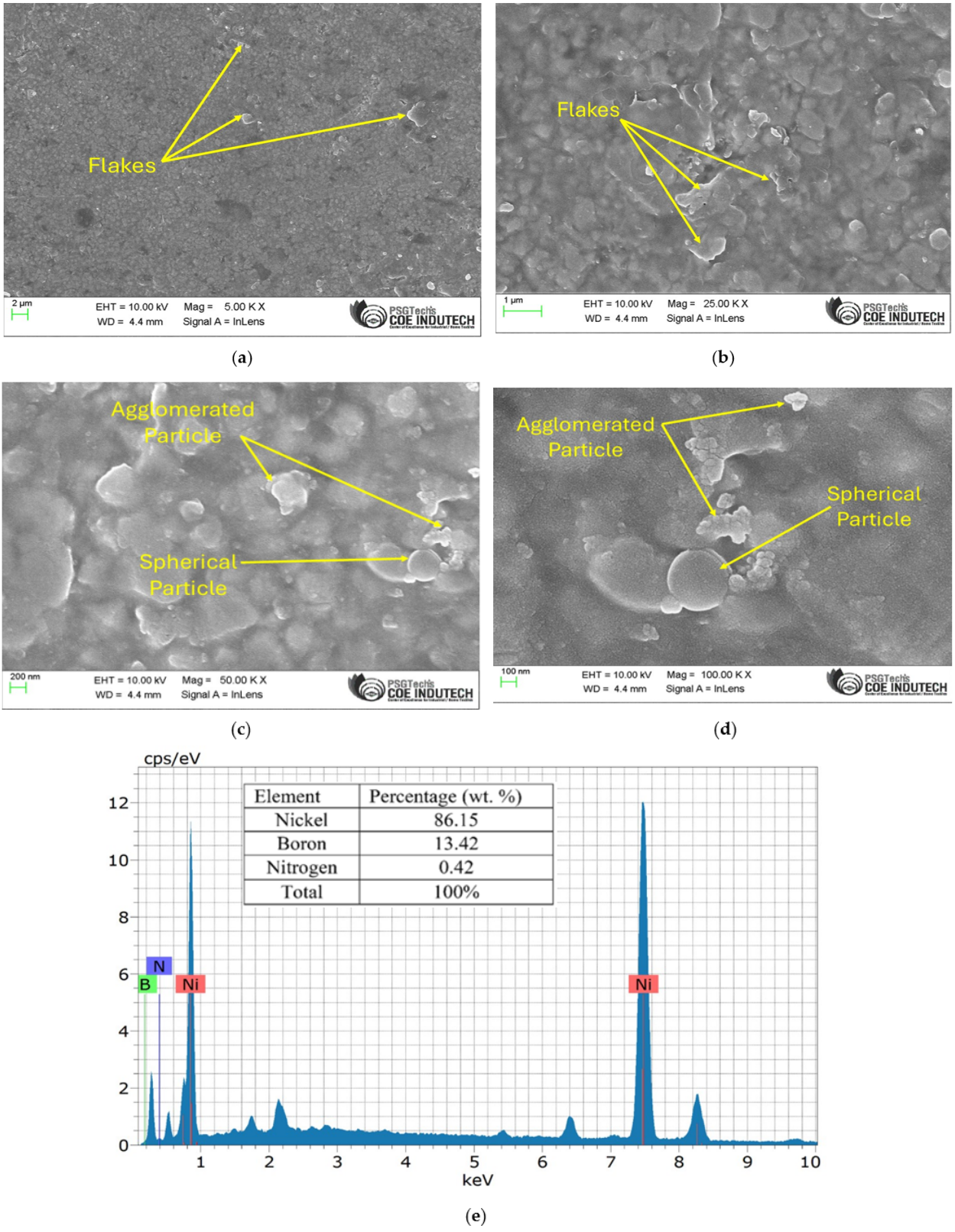


Figure 2. (**a**–**d**) Surface morphology of Ni–hBN coated sample. (**e**) EDX and elements of Ni–hBN-coated sample.

When the current density ratio equals 2 [51] and the total plating time is 5 min [52], the coating thickness of the sample as per ISO 1463:2004 standards [49] was 4 µm which can be witnessed in Figure 3. The average crystallite size was determined for the composite layers using Scherrer's equation reminded in Section 2.2. The average crystal size of the

AD sample was found to be 17.86 nm while the average crystal size of the HT sample was found to be 19.6 nm. The findings suggest that crystal size marginally increased upon heat treatment.

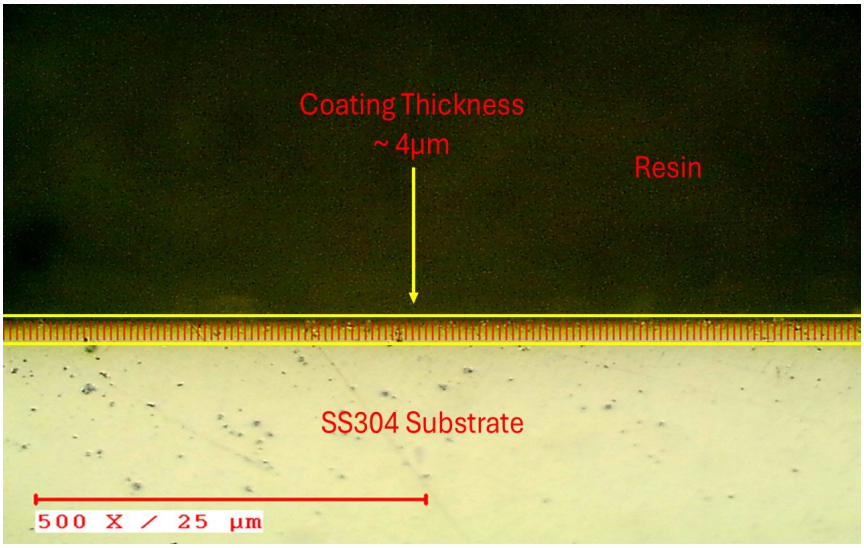


Figure 3. Coating thickness.

The XRD analysis for AD and HT Ni-hBN composite coatings is shown in Figure 4 where the curve displayed characteristic peaks corresponding to both the Ni and hBN phases. It can be summarized that in the AD state, Ni peaks primarily arise from the face-centered cubic (FCC) structure of nickel with peaks at 2θ = 42.722° (111), 51.8° (200), and 76.4° (220) indicating the crystalline nature of the nickel which matches ICCID number 98-002-7986. The Ni peaks may shift or broaden due to changes in lattice parameters or crystallite size, reflecting thermal effects. The intensity of the hBN (002) peak may decrease or shift, depending on the heat treatment's effect on hBN, including potential decomposition or phase transformation. For example, the peak of the AD sample at 2θ = 42.722° corresponds to a monoclinic structure which suggests that the coating initially has an ordered but non-hexagonal phase. However, after heat treatment (HT), the first peak shifts to 2θ = 42.766° which indicates the formation of a hexagonal structure. This shift in the peak position suggests that the heat treatment has induced a phase transition from a monoclinic to a more stable hexagonal phase in the coating, likely due to changes in crystallinity and thermal effects on the coating's microstructure. The hBN phase is marked by a distinct peak around 2θ~26°, corresponding to the (002) plane of hexagonal boron nitride. Upon heat treatment (HT), the XRD pattern can show changes in the crystallinity and phase composition of both phases.

Upon measuring the surface roughness, it was found that surface roughness of the Ni-hBN-coated sample was 0.43 ± 0.08 µm, while a bare surface has a surface roughness of 0.48 µm. Coating of Ni-hBN over the substrate reduced the surface roughness where the addition of hBN into the Ni matrix changed the electro-crystallization mechanism and resulted in a smoother surface and homogenous surface morphology with a lower surface roughness value of 0.43 µm [53]. Meanwhile, when the coated sample is heat-treated, the surface roughness is increased further to 0.47 ± 0.02 µm. However, the surface roughness of the HT sample is less than the one reported by Leon et al. [54]. In his research on Ni–P–hBN composite autocatalytic-coated 316L stainless steel, they could achieve the surface roughness of 0.595 µm. The average crystal size, hardness, surface roughness, average coefficient friction, wear rate, and corrosion rate of the AD sample and HT sample are evaluated and shown in Table 2.

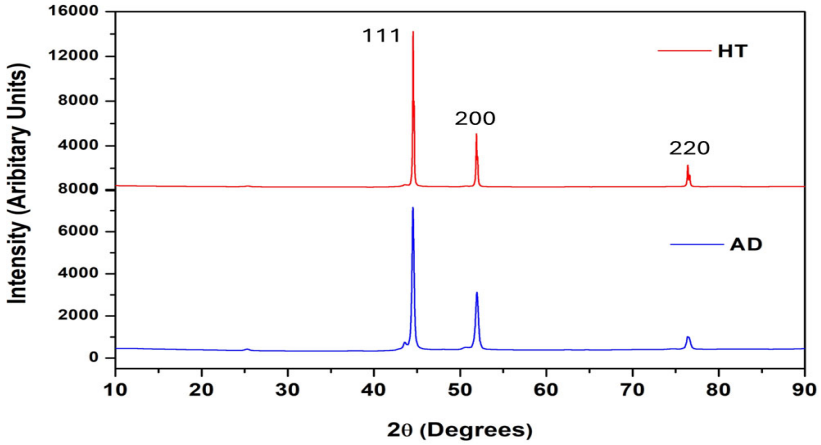


Figure 4. XRD analysis of AD and HT Ni-hBN composite coatings.

Table 2. Properties of Ni-hBN-coated samples with and without heat treatment.

Sample	Avg. Cry. Size nm	Microhardness HV	Surface Roughness μm	Avg. CoF	Volume Loss mm^3	Wear Rate mm^3/N-m	Corrosion Potential V	Corrosion Current Density A/cm^2	Corrosion Rate mm/yr	Corrosion Protection Efficiency
Bare surface [18]	-	250.0	0.48	0.845	4.13×10^{-6}	3.311×10^{-5}	0.166	2.19×10^{-4}	1.675	-
AD	17.86	372.6 ± 5.0	0.43 ± 0.08	0.487	3.34×10^{-7}	2.980×10^{-6}	−0.050	8.42×10^{-6}	0.062	96.23
HT	19.60	459.6 ± 7.2	0.47 ± 0.02	0.310	7.64×10^{-8}	6.800×10^{-7}	−0.650	1.12×10^{-5}	0.083	94.99

3.1. Microhardness and Wear Characteristics

Microhardness of the AD sample was 372.6 ± 5.0 HV, 49% higher compared to the bare surface. The enhanced microhardness of the nanocomposite coating could be attributed to three factors: (i) due to dispersion strengthening of the hBN nanoparticles, (ii) hBN nanoparticles in the composite must have restricted the growth of the nickel matrix, which subsequently reduced crystallite sizes, and (iii) obstructing the displacement and sliding boundary by hBN nanoparticles. The HT sample has an enhanced hardness of 459.6 ± 7.2 HV, which is 83.84% higher compared to the bare surface. The HT sample has a grain size of 19.6 nm compared to the as-deposited surface, which is 17.86 nm. This is because the heat treatment has allowed the grains to grow more extensively, and upon quenching in oil, the larger grains began to contract. Though it contracts, the grain size of the HT sample was limited to higher than the AD sample. Moreover, the grains were closely packed, providing resistance to indentation. It seems like a more complex surface compared to the AD sample. The average coefficient of friction (CoF) of the AD sample was 0.487 which is 42.4% less than the bare surface. This could be attributed by the presence of nano hBN which acts as a self-lubricant, hence enhancing its tribological characteristic. Microhardness and the fine-grained structure of the HT sample must have affected the wear characteristic and coefficient of friction.

Upon analyzing the SEM results of worn-out surfaces of AD samples as shown in Figure 5a–d and HT samples as shown in Figure 5e–h, we could understand that abrasive particles could have removed nickel deposits by plowing to create grooves. Significant distortion of coating materials resulted in surface flattening and reduced surface roughness, reducing its roughness as witnessed in Figure 5a–d. This could be the reason for the low frictional coefficient and high wear resistance. To conclude, the Ni-hBN coating tends to improve wear characteristics than uncoated samples due to the load-bearing characteristic. This is in accordance with Archard's law where the wear rate and weight loss of the material was influenced by its microhardness [55].

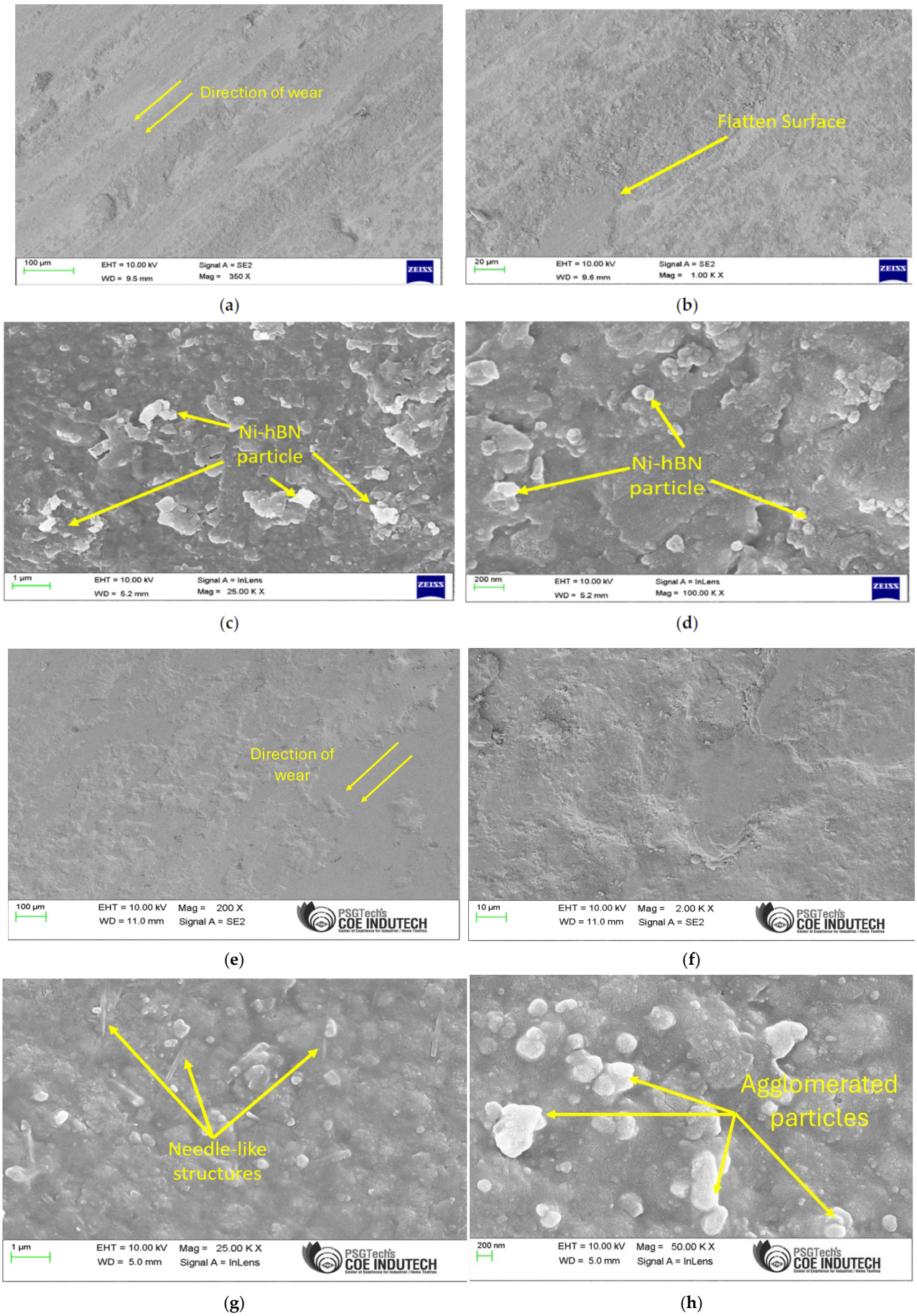


Figure 5. Worn surfaces: (**a**–**d**) AD samples (**e**–**h**) HT samples.

3.2. Corrosion Resistance

The potentiodynamic polarization of the Ni-hBN composite-coated sample was examined with electrochemical impedance spectroscopy. Figure 6 and Table 2 shows a Tafel extrapolation plot in which we could witness a low corrosion rate in the HT sample due to dispersion of hBN particles in the Ni matrix. The Ni-hBN AD sample demonstrates significantly enhanced corrosion resistance, as evidenced by its lower corrosion current density (8.42×10^{-6} A/cm^2) from Table 2 compared to the bare and heat-treated (HT) surfaces. This improvement is primarily attributed to the optimized pulse-reverse current deposition parameters—such as frequency, duty cycle, plating time, and polarity ratio—which facilitate the formation of a denser and more uniform composite coating. The incorporation of nano-sized hexagonal boron nitride (hBN) particles into the nickel matrix modifies the preferred crystallographic orientation of the nickel grains, promoting grain refinement and structural changes that enhance the coating's compactness [56]. These nanoparticles act as physical barriers, effectively sealing surface imperfections like micropores, voids, and cracks, thereby reducing the permeability of corrosive agents such as NaCl [57]. Furthermore, the uniform distribution of hBN particles along grain boundaries during electroplating minimizes structural defects and contributes to a less permeable, more protective surface [58,59]. Collectively, these effects result in a composite coating with superior corrosion resistance due to both its electrochemical stability and its physical integrity. The corrosion rate of the AD sample is found to be 0.062 mm/year which seems lesser than findings reported by Gyawali et al. [3]. In his work, corrosion rate was reported as 0.074 mm/year when 5 g/L hBN dispersed in the bath. As the corrosion protection efficiency of the AD sample is 96.23%, the method employed in this research could protect the substrate very well with superior corrosion resistance. The corrosion rate of the HT sample is 0.083 mm/year in 3.5% NaCl neutral solution. The AD coating produced a corrosion current density of 10^{-6} A/cm^2, which can be a vibrant replacement for hard chromium coating [60].

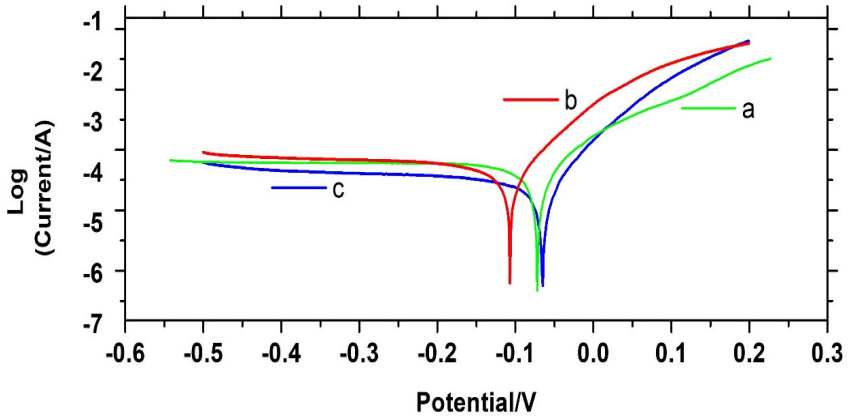


Figure 6. Tafel plots of (**a**) bare surface [18], (**b**) as-deposited Ni-hBN composite-coated sample (**c**) heat-treated Ni-hBN composite-coated sample.

Table 3 provides a comprehensive comparison between the current research and other published results. We conclude that the Ni-hBN composite coating followed by heat treatment would be an excellent method to provide a protected surface to the SS304 substrate. We suggest further research into elevated temperatures with various cooling mediums or cryogenic environment in the future.

Table 3. Comparison of hardness, wear rate, and corrosion rate of Ni-hBN coatings obtained in the present study with conventional coatings reported in other studies.

Substrate	Coating	AD/HT	Microhardness HV	CoF	Wear Rate mm^3/N-m	Corrosion Rate mm/yr	Reference
SS 304	Ni-TiO_2	HT	446.4	0.200	3.20×10^{-7}	0.091	[18]
C45E steel	Ni-B	AD	429	0.896	n/a	n/a	[41]
Nickel	Ni-B	AD	189	0.930	0.02×10^{-3}	n/a	[43]
AISI 316L	Electroless-Ni-P-BN (h)	AD	456	n/a	1.24×10^{-6}	n/a	[54]
SS 304	Ni-hBN	AD	372.6	0.487	2.98×10^{-6}	0.062	Present work
SS 304	Ni-hBN	HT @ 400 °C	459.6	0.310	6.80×10^{-7}	0.083	Present work
AISI 316L	Ni-P-BN	HT @ 400 °C	n/a	0.200	4.87×10^{-7}	n/a	[61]
Brass	Ni-cBN	AD	480.0	0.580	n/a	n/a	[62]
Steel	Ni-P	HT @ 400 °C	900.0–1100.0	~0.460	3.50×10^{-5}	n/a	[63]
Steel	Hard chrome coating	AD	980.0–1050.0	~0.560	4.20×10^{-5}	n/a	[63]
Steel	Ni-W/PTFE	AD	459.6	0.420	3.30×10^{-7}	n/a	[64]
SSAB Domex 350LA	HVAF spraying-Cr_3C_2–NiCr -hBN	AD	997 with 309 µm coating thickness	0.260	1.50×10^{-5}	n/a	[65]
SS304	Laser clad Ni60/h-BN	HT	765.0	0.390	n/a	n/a	[66]
LM26	Ni-G	AD	275.2	0.370	n/a	0.062	[67]

4. Conclusions

This study systematically evaluated the effect of an Ni-hBN composite coating on the mechanical, tribological, and corrosion properties of SS304 stainless steel, with a focus on the influence of post-deposition heat treatment. The key findings are summarized below:

- The Ni-hBN coating significantly improved the microhardness of the substrate. The as-deposited sample exhibited a 48% increase in hardness compared to the bare SS304 surface, while the heat-treated (HT) sample showed an even greater improvement of 83.8%, attributed to the formation of densely packed grains during thermal treatment followed by quenching.
- The as-deposited coating exhibited finer grain structures than the uncoated substrate. After heat treatment, the average grain size increased slightly from 17.86 nm (as-deposited) to 19.6 nm, explained by the expansion–contraction mechanism induced by thermal cycling.
- The coated samples demonstrated marked improvements in both wear resistance and corrosion protection relative to the uncoated substrate. These enhancements were primarily attributed to the synergistic lubricating behavior of hexagonal boron nitride (hBN) within the Ni matrix.
- The corrosion rate of the as-deposited Ni-hBN coating was measured at 0.062 mm/year, a value notably lower than those reported in existing literature. The coating provided an overall corrosion protection efficiency of 96.23%.

In conclusion, this research establishes pulse-reverse electrodeposition as a reliable technique for fabricating Ni-hBN composite coatings with superior surface properties. The incorporation of hBN not only enhances the wear and corrosion resistance of SS304 but also reduces reliance on environmentally harmful coatings like hard chrome. Heat treatment following deposition further optimizes mechanical and tribological performance, making the approach particularly promising for high-performance applications in the automotive and aerospace industries.

Author Contributions: Conceptualization, S.V. and A.C.; methodology, K.M.; software, K.V. and K.M.; validation, S.V., S.M.S. and E.N.; formal analysis, G.F.; investigation, S.V.; resources, S.V.; data curation, E.N.; writing—original draft preparation, S.V.; writing—review and editing, E.N. and G.F.;

visualization, G.F.; supervision, S.V.; project administration, S.V. All authors have read and agreed to the published version of the manuscript.

Funding: This research received no external funding.

Data Availability Statement: The original contributions presented in this study are included in the article. Further inquiries can be directed to the corresponding author(s).

Conflicts of Interest: The authors declare no conflicts of interest. The funders had no role in the design of the study; in the collection, analyses, or interpretation of data; in the writing of the manuscript; or in the decision to publish the results.

Abbreviations

The following abbreviations are used in this manuscript:

AD	As-deposited
Al_2O_3	Aluminum dioxide
B	Boron
Ca/P	Calcium-to-phosphorus ratio
Co	Cobalt
CoF	Coefficient of friction
Cr_2O_3	Chromium oxide
Cu K-α	Copper K-α x-ray
EDX	Energy dispersive X-ray spectrometry
FCC	Face-centered cubic
Fe_2O_3	Ferric oxide
FESEM	Field emission scanning electron microscopy
GO	Graphene oxide
HVAF	High-velocity air fuel
hBN	Hexagonal boron nitride
HCl	Hydrochloric acid
H_2SO_4	Dihydrogen sulfate (sulfuric acid)
HT	Heat-treated
MMC	Metal matrix composite
Mo	Molybdenum
N	Nitrogen
NaCl	Sodium chloride
Ni	Nickel
P	Phosphorus
PRED	Pulse-reverse electrodeposition
SCE	Saturated calomel electrode
SDS	Sodium dodecyl sulfate
SEM	Scanning electron microscopy
SiC	Silicon carbide
Si_3N_4	Silicon nitride
SS304	304 stainless steel
Ti	Titanium
TiO_2	Titanium dioxide
WC	Tungsten carbide
XRD	X-ray diffraction
ZrO_2	Zirconium dioxide

References

1. Pradhan, K.K.; Matawale, C.R. Heat treatment analysis of SS304 for gas turbine application. *Mater. Today Proc.* **2020**, *33*, 5734–5739. [CrossRef]

2. Ouyang, J.H.; Li, Y.F.; Zhang, Y.Z.; Wang, Y.M.; Wang, Y.J. High-temperature solid lubricants and self-lubricating composites: A critical review. *Lubricants* **2022**, *10*, 177. [CrossRef]
3. Gyawali, G.; Adhikari, R.; Kim, H.S.; Cho, H.-B.; Lee, S.W. Effect of h-BN Nanosheets Codeposition on Electrochemical Corrosion Behavior of Electrodeposited Nickel Composite Coatings. *ECS Electrochem. Lett.* **2012**, *2*, C7–C10. [CrossRef]
4. Bouzit, F.Z.; Nemamcha, A.; Moumeni, H.; Rehspringer, J.L. Morphology and Rietveld analysis of nanostructured Co-Ni electrodeposited thin films obtained at different current densities. *Surf. Coat. Technol.* **2017**, *315*, 172–180. [CrossRef]
5. Khorsand, S.; Raeissi, K.; Ashrafizadeh, F.; Arenas, M.A.; Conde, A. Corrosion behaviour of super-hydrophobic electrodeposited nickel–cobalt alloy film. *Appl. Surf. Sci.* **2016**, *364*, 349–357. [CrossRef]
6. Zhang, F.; Yao, Z.; Moliar, O.; Tao, X.; Yang, C. Nanocrystalline Ni coating prepared by a novel electrodeposition. *J. Alloys Compd.* **2020**, *830*, 153785. [CrossRef]
7. Bigos, A.; Janusz-Skuza, M.; Szczerba, M.J.; Kot, M.; Zimowski, S.; Dębski, A.; Beltowska-Lehman, E. The effect of heat treatment on the microstructural changes in electrodeposited Ni-Mo coatings. *J. Mater. Process. Technol.* **2020**, *276*, 116397. [CrossRef]
8. Yin, K.-M. Duplex diffusion layer model for pulse with reverse plating. *Surf. Coat. Technol.* **1997**, *88*, 162–164. [CrossRef]
9. Bucur, A.I.; Linul, E.; Taranu, B.-O. Hydroxyapatite coatings on Ti substrates by simultaneous precipitation and electrodeposition. *Appl. Surf. Sci.* **2020**, *527*, 146820. [CrossRef]
10. Tohidi, P.M.S.; Safavi, M.S.; Etminanfar, M.; Khalil-Allafi, J. Pulsed electrodeposition of compact, corrosion resistant, and bioactive HAp coatings by application of optimized magnetic field. *Mater. Chem. Phys.* **2020**, *254*, 123511. [CrossRef]
11. Gopi, D.; Indira, J.; Kavitha, L. A comparative study on the direct and pulsed current electrodeposition of hydroxyapatite coatings on surgical grade stainless steel. *Surf. Coat. Technol.* **2012**, *206*, 2859–2869. [CrossRef]
12. Drevet, R.; Benhayoune, H.; Wortham, L.; Potiron, S.; Douglade, J.; Laurent-Maquin, D. Effects of pulsed current and H2O2 amount on the composition of electrodeposited calcium phosphate coatings. *Mater. Charact.* **2010**, *61*, 786–795. [CrossRef]
13. Li, J.; Lin, O.; Cheng, C.; Wang, W.; Xu, C.; Ren, L. Fabrication of a Ni/SiC composite coating on steel surface with excellent corrosion inhibition performance. *J. Mater. Process. Technol.* **2021**, *290*, 116987. [CrossRef]
14. Chang, L.M. Diffusion layer model for pulse reverse plating. *J. Alloys Compd.* **2008**, *466*, L19–L22. [CrossRef]
15. Li, J.; An, Z.; Wang, Z.; Toda, M.; Ono, T. Pulse-Reverse Electrodeposition and Micromachining of Graphene–Nickel Composite: An Efficient Strategy toward High-Performance Microsystem Application. *ACS Appl. Mater. Interfaces* **2016**, *8*, 3969–3976. [CrossRef]
16. Cherevko, S.; Kulyk, N.; Chung, C.-H. Pulse-reverse electrodeposition for mesoporous metal films: Combination of hydrogen evolution assisted deposition and electrochemical dealloying. *Nanoscale* **2012**, *4*, 568–575. [CrossRef]
17. Gurrappa, I.; Binder, L. Electrodeposition of nanostructured coatings and their characterization—A review. *Sci. Technol. Adv. Mater.* **2008**, *9*, 043001. [CrossRef]
18. Suresh, V.; Jegan, A. Experimental studies on wear and corrosion resistance of pulse electrodeposited Ni-TiO_2 nanocomposite coatings on AISI 304 stainless steel. *Mater. Res. Express* **2022**, *9*, 126401. [CrossRef]
19. Jegan, A.; Venkatesan, R.; Arunachalam, R. Mechanical properties of Ni-nano-Al_2O_3 composite coatings on AISI 304 stainless steel by pulsed electrodeposition. *Sci. Eng. Compos. Mater.* **2014**, *21*, 351–358. [CrossRef]
20. Jegan, A. Pulse eletrodeposition of Ni/nano-Al_2O_3 composite coatings on cast iron cylinder liner. *Mater. Res.* **2018**, *21*, e20180060. [CrossRef]
21. Joshua, D.R.; Jegan, A.; Srinivasan, A. Multi Objective Optimization of Pulse Electrodeposition of nano Ni-TiO_2 and Ni-Al_2O_3 Coating on Inconel 617. *Int. J. Electrochem. Sci.* **2022**, *17*, 220418. [CrossRef]
22. Natarajan, P.; Jegan, A.; Ganesh, S.S. Development of numerical model for predicting the characteristics of Ni–SiC nano composite coatings on AISI 1022 substrate. *Mater. Res. Express* **2019**, *6*, 085048. [CrossRef]
23. Chakraborty, S.; Langford, N.; Kohl, Y.; Varsou, D.D.; Stokes, W.; Papaioannou, E.; Wien, S.; Britton, A.; Ibrahim, B.; Afantitis, A.; et al. Are Ni–SiC nanoparticle electroplated coatings a safer alternative to hard chromium? A comprehensive aging, toxicity, and in silico study to assess safety by design. *Environ. Sci. Nano* **2025**, *12*, 894–908. [CrossRef]
24. Zellele, D.M.; Yar-Mukhamedova, G.S.; Rutkowska-Gorczyca, M. A Review on Properties of Electrodeposited Nickel Composite Coatings: Ni-Al_2O_3, Ni-SiC, Ni-ZrO_2, Ni-TiO_2 and Ni-WC. *Materials* **2024**, *17*, 5715. [CrossRef] [PubMed]
25. Ganesh, S.S.; Jegan, A. Response surface methodology optimization of pulse electrodeposited Ni-nano SiC coatings on Al 7075 substrate. *J. Ceram. Process Res.* **2023**, *24*, 486–494.
26. Dadvand, M.; Savadogo, O. Effect of hBN on Corrosion and Wear Performances of DC Electrodeposited NiW and NiW–SiC on Brass Substrates. *Coatings* **2022**, *12*, 1011. [CrossRef]
27. Lai, L.; Qian, F.; Bi, Y.; Niu, B.; Yu, G.; Li, Y.; Ding, G. Advancements in the Preparation and Application of Ni-Co System (Alloys, Composites, and Coatings): A Review. *Nanomaterials* **2025**, *15*, 312. [CrossRef]
28. Nemane, V.; Misra, D.; Chatterjee, S. Development and Characterization of Nickel-Based Self-Lubricating Electroless Composite Coatings Involving SiC and hBN. *J. Mater. Eng. Perform.* **2025**. [CrossRef]

29. Eskandari, M.; Shanaghi, A.; Kamani, M.; Niari, M.A. Effect of nano-metal oxides (ZnO, Al_2O_3, CuO, and TiO_2) on the corrosion behavior of a nano-metal oxide/epoxy coating applied on the copper substrate in the acidic environment. *Appl. Nanosci.* **2021**, *11*, 1605–1615. [CrossRef]
30. Sharma, A.; Singh, A.K. Electroless Ni-P and Ni-P-Al_2O_3 Nanocomposite Coatings and Their Corrosion and Wear Resistance. *J. Mater. Eng. Perform.* **2013**, *22*, 176–183. [CrossRef]
31. Bisht, A.K.; Vaishya, R.O.; Walia, R.S.; Singh, G. Nitrides ceramic coatings for tribological applications: A journey from binary to high-entropy compositions. *Ceram. Int.* **2024**, *50*, 8553–8585. [CrossRef]
32. Siddaiah, A.; Kumar, P.; Henderson, A.; Misra, M.; Menezes, P.L. Surface energy and tribology of electrodeposited Ni and Ni–graphene coatings on steel. *Lubricants* **2019**, *7*, 87. [CrossRef]
33. Guan, T.; Zhang, N. Recent Advances in Electrodeposition of Nickel-Based Nanocomposites Enhanced with Lubricating Nanoparticles. *Nanomanuf. Metrol.* **2024**, *7*, 25. [CrossRef] [PubMed]
34. Ziyamukhamedova, U.; Wasil, S.; Kumar, S.; Sehgal, R.; Wani, M.F.; Singh, C.S.; Tursunov, N.; Gupta, H.S. Investigating friction and antiwear characteristics of organic and synthetic oils using h-bn nanoparticle additives: A tribological study. *Lubricants* **2024**, *12*, 27. [CrossRef]
35. Zhao, M.; Li, J.; Li, C.; Li, Y.; Zhang, X. Study on Current-Carrying Friction Characteristics and Corrosion Resistance of Carbon Brush/Collector Ring by Copper–Graphene Electrodeposition Process. *Lubricants* **2025**, *13*, 162. [CrossRef]
36. Gao, Q.; Liu, S.; Hou, K.; Li, Z.; Wang, J. Graphene-based nanomaterials as lubricant additives: A review. *Lubricants* **2022**, *10*, 273. [CrossRef]
37. Makhesana, M.A.; Patel, K.M.; Bagga, P.J. Evaluation of surface roughness, tool wear and chip morphology during machining of nickel-based alloy under sustainable hybrid nanofluid-MQL strategy. *Lubricants* **2022**, *10*, 315. [CrossRef]
38. Kumar, J.S.; Jegan, A. Tribological Investigation of Nickel Nanocomposite Coated Piston Rings Reinforced with Multi-Walled Carbon Nanotubes. *Int. J. Electrochem. Sci.* **2021**, *16*, 210429. [CrossRef]
39. Fang, H.; Bai, S.-L.; Wong, C.P. 'White graphene'—Hexagonal boron nitride based polymeric composites and their application in thermal management. *Compos. Commun.* **2016**, *2*, 19–24. [CrossRef]
40. Zuo, K.; Wang, W.; Deshmukh, A.; Jia, S.; Guo, H.; Xin, R.; Elimelech, M.; Ajayan, P.M.; Lou, J.; Li, O. Multifunctional nanocoated membranes for high-rate electrothermal desalination of hypersaline waters. *Nat. Nanotechnol.* **2020**, *15*, 1025–1032. [CrossRef]
41. Bányai, K.; Czagány, M.; Kovács, S.; Bognár, G. Characterisation of Tribological Properties and Morphologies of Ni-P and Ni-B Coatings. *Lubricants* **2025**, *13*, 168. [CrossRef]
42. Rajagopal, I. Electroless and electrodeposition of nickel boron composites. *Bull. Mater. Sci.* **1983**, *5*, 323–331. [CrossRef]
43. Raghavendra, C.R.; Basavarajappa, S.; Sogalad, I.; Kumar, S. A review on Ni based nano composite coatings. *Mater. Today Proc.* **2021**, *39*, 6–16. [CrossRef]
44. Ahmadkhaniha, D.; Eriksson, F.; Leisner, P.; Zanella, C. Effect of SiC particle size and heat-treatment on microhardness and corrosion resistance of NiP electrodeposited coatings. *J. Alloys Compd.* **2018**, *769*, 1080–1087. [CrossRef]
45. Kiran, K.U.V.; Arora, A.; Sunil, B.R.; Dumpala, R. Effect of heat treatment on the temperature dependent wear characteristics of electroless Ni–P–BN(h) composite coatings. *SN Appl. Sci.* **2020**, *2*, 1101. [CrossRef]
46. Jiang, J.; Chen, H.; Zhu, L.; Qian, W.; Han, S.; Lin, H.; Wu, H. Effect of heat treatment on structures and mechanical properties of electroless Ni–P–GO composite coatings. *RSC Adv.* **2016**, *6*, 109001–109008. [CrossRef]
47. *ASTM G99-17*; Standard Test Method for Wear Testing with a Pin-On-Disk Apparatus. ASTM: West Conshohocken, PA, USA, 2023. [CrossRef]
48. Ünal, E.; Karahan, I.H. Effects of ultrasonic agitation prior to deposition and additives in the bath on electrodeposited Ni-B/hBN composite coatings. *J. Alloys Compd.* **2018**, *763*, 329–341. [CrossRef]
49. *ISO 1463:2004*; Metallic and Oxide Coatings—Measurement of Coating Thickness—Microscopical Method. International Organization for Standardization: Geneva, Switzerland, 2004.
50. *ASTM G106-89*; Standard Practice for Verification of Algorithms and Equipment for Electrochemical Impedance Measurements. ASTM: West Conshohocken, PA, USA, 2023. [CrossRef]
51. Ismail, M.I. Periodic reverse current electroplating and surface finishing. *J. Appl. Electrochem.* **1979**, *9*, 407–410. [CrossRef]
52. Canning, W. *The Canning Handbook: Surface Finishing Technology, Integrated Design*; Springer: Berlin/Heidelberg, Germany, 1982.
53. Awasthi, S.; Pandey, C.P.; Balani, K. Synergistic role of carbonaceous reinforcements on multi length scale tribology of electrophoretically deposited nickel-boron nitride coatings. *Mater. Res. Bull.* **2018**, *99*, 61–72. [CrossRef]
54. León, O.A.; Staia, M.H.; Hintermann, H.E. Wear mechanism of Ni–P–BN(h) composite autocatalytic coatings. *Surf. Coat. Technol.* **2005**, *200*, 1825–1829. [CrossRef]
55. Shahri, Z.; Allahkaram, S.R. Effect of particles concentration and current density on the cobalt/hexagonal boron nitride nanocomposite coatings properties. *Iran. J. Mater. Sci. Eng.* **2012**, *9*, 1–7.
56. Feng, Q.; Li, T.; Teng, H.; Zhang, X.; Zhang, Y.; Liu, C.; Jin, J. Investigation on the corrosion and oxidation resistance of Ni–Al_2O_3 nano-composite coatings prepared by sediment co-deposition. *Surf. Coat. Technol.* **2008**, *202*, 4137–4144. [CrossRef]

57. Ali, M.R.; Chowdhury, M.A.; Shahin, M.; Rahman, M.M.; Ali, M.O.; Gafur, M.A. Multi-physical and anti-corrosion properties of graphene-reinforced epoxy nanocomposite coatings for industrial applications. *Arab. J. Chem.* **2024**, *17*, 105424. [CrossRef]
58. Kasturibai, S.; Kalaignan, G.P. Characterizations of electrodeposited Ni–CeO_2 nanocomposite coatings. *Mater. Chem. Phys.* **2014**, *147*, 1042–1048. [CrossRef]
59. Wang, Y.; Wang, S.-J.; Shu, X.; Gao, W.; Lu, W.; Yan, B. Preparation and property of sol-enhanced Ni–B–TiO_2 nano-composite coatings. *J. Alloys Compd.* **2014**, *617*, 472–478. [CrossRef]
60. Kandeva, M.; Zagorski, M.; Nikolić, R.; Stojanović, B.; But, A.; Botko, F.; Piteľ, J.; Vencl, A. Friction Properties of the Heat-Treated Electroless Ni Coatings Embedded with c-BN Nanoparticles. *Coatings* **2022**, *12*, 1008. [CrossRef]
61. León, O.A.; Staia, M.H.; Hintermann, H.E. Influence of the heat treatment on the tribological behavior of a Ni–P–BN(h) autocatalytic composite coating. *Surf. Coat. Technol.* **1999**, *120–121*, 641–645. [CrossRef]
62. Pompei, E.; Magagnin, L.; Lecis, N.; Cavallotti, P.L. Electrodeposition of nickel–BN composite coatings. *Electrochim. Acta* **2009**, *54*, 2571–2574. [CrossRef]
63. Wang, L.; Gao, Y.; Xue, Q.; Liu, H.; Xu, T. A novel electrodeposited Ni–P gradient deposit for replacement of conventional hard chromium. *Surf. Coat. Technol.* **2006**, *200*, 3719–3726. [CrossRef]
64. Karadag, A.; Duru, E.; Uysal, M.; Akbulut, H.; Coban, A. Tribological performance of Ni-W/PTFE composite coating via pulse electrodeposition. *Therm. Sci.* **2022**, *26*, 2885–2893. [CrossRef]
65. Ganvir, A.; Jahagirdar, A.R.; Mulone, A.; Örnfeldt, L.; Björklund, S.; Klement, U.; Joshi, S. Novel utilization of liquid feedstock in high velocity air fuel (HVAF) spraying to deposit solid lubricant reinforced wear resistant coatings. *J. Mater. Process. Technol.* **2021**, *295*, 117203. [CrossRef]
66. Lu, X.L.; Liu, X.B.; Yu, P.C.; Zhai, Y.J.; Qiao, S.J.; Wang, M.D.; Wang, Y.G.; Chen, Y. Effects of heat treatment on microstructure and mechanical properties of Ni60/h-BN self-lubricating anti-wear composite coatings on 304 stainless steel by laser cladding. *Appl. Surf. Sci.* **2015**, *355*, 350–358. [CrossRef]
67. Velayudham, S.; Natarajan, E.; Markandan, K.; Anbuchezhiyan, G.; Franz, G.; Mohan, D.G. Ni-Graphene Nanocomposite Coated Aluminum LM26 Substrate: Investigation Summary on Microhardness, Wear, and Corrosion Resistance. *Arab. J. Sci. Eng.* **2025**, 1–11. [CrossRef]

Disclaimer/Publisher's Note: The statements, opinions and data contained in all publications are solely those of the individual author(s) and contributor(s) and not of MDPI and/or the editor(s). MDPI and/or the editor(s) disclaim responsibility for any injury to people or property resulting from any ideas, methods, instructions or products referred to in the content.